



Published in final edited form as:

*ACS Biomater Sci Eng.* 2020 July 13; 6(7): 4166–4178. doi:10.1021/acsbiomaterials.0c00131.

## Mixed Composition Microribbon Hydrogels Induce Rapid and Synergistic Cartilage Regeneration by Mesenchymal Stem Cells in 3D *via* Paracrine Signaling Exchange

**Courtney Gegg,**

Department of Bioengineering, Stanford University Schools of Engineering and Medicine, Stanford, California 94305, United States

**Xinming Tong,**

Department of Orthopedic Surgery, Stanford University School of Medicine, Stanford, California 94305, United States

**Fan Yang**

Department of Bioengineering and Orthopedic Surgery, Stanford University Schools of Engineering and Medicine, Stanford, California 94305, United States

### Abstract

Hydrogels are widely used matrices for mesenchymal stem cell (MSC)-based cartilage regeneration but often result in slow cartilage deposition with inferior mechanical strength. We recently reported a gelatin-based microribbon ( $\mu$ RB) scaffold, which contains macroporosity and substantially enhances the speed of cartilage formation by MSCs in 3D. However, our previous method cannot be used to fabricate different polymers into  $\mu$ RBs, and the effects of varying  $\mu$ RB compositions on MSC cartilage regeneration in 3D remain unknown. Here, we report a method that allows fabricating different polymers [gelatin, chondroitin sulfate, hyaluronic acid, and polyethylene glycol (PEG)] into  $\mu$ RB structures, which can be mixed in any ratio and cross-linked into 3D scaffolds in a modular manner. Mixing glycosaminoglycan  $\mu$ RBs with gelatin or PEG  $\mu$ RBs induced great synergy, resulting in fast cartilage deposition. After only 3 weeks of culture, leading mixed  $\mu$ RB composition reached high compressive strength on par with native cartilage. Such synergy can be recapitulated *via* exchange of soluble factors secreted by MSCs seeded in different  $\mu$ RB compositions in a dose-dependent manner. Tuning the ratio of mixed  $\mu$ RB compositions allowed further optimization of the quantity and speed of cartilage regeneration by MSCs. Together, our results validate mixed  $\mu$ RB compositions as a novel biomaterial tool for

---

**Corresponding Author: Fan Yang** – Phone: (650) 725-7128, fanyang@stanford.edu.

The authors declare no competing financial interest.

#### ASSOCIATED CONTENT

##### Supporting Information

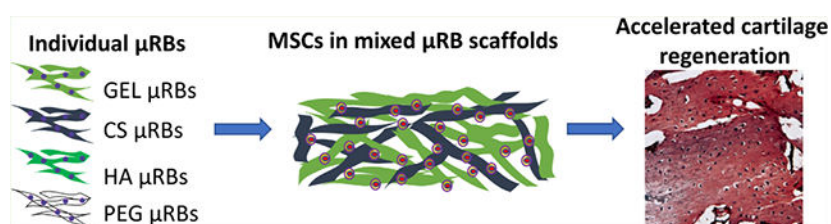
The Supporting Information is available free of charge at <https://pubs.acs.org/doi/10.1021/acsbiomaterials.0c00131>.

Cyclic compression and shear testing; day 1 individual acellular scaffold compressive moduli; day 21 macroscopic histology of individual and mixed  $\mu$ RB constructs; day 21 histology of acellular individual and mixed  $\mu$ RB scaffolds; swelling and BSA release from individual  $\mu$ RB scaffolds; day 21 individual  $\mu$ RB scaffold dimensions; mechanosensing gene analysis of individual  $\mu$ RB scaffolds; confocal imaging of MSCs within mixed  $\mu$ RB scaffold; and chondrogenic gene expression in individual  $\mu$ RB scaffolds (PDF)

Complete contact information is available at: <https://pubs.acs.org/10.1021/acsbiomaterials.0c00131>

inducing synergy and accelerating MSC-based cartilage regeneration with biomimetic mechanical properties through paracrine signal exchange.

## Graphical Abstract



## Keywords

scaffolds; hydrogels; tissue engineering; stem cells; cartilage

## 1. INTRODUCTION

Hydrogels are widely used as 3D matrices to guide stem cell differentiation for tissue-engineering applications because of their injectability and tunable properties.<sup>1,2</sup> Both natural and synthetic polymers have been fabricated into hydrogels with demonstrated promise for supporting stem cell-based cartilage tissue engineering.<sup>3–9</sup> However, several key bottlenecks remain. First, cartilage formation in conventional hydrogels is often delayed and restricted to pericellular regions because of the physical restriction of the nanoporous polymer network. To overcome the physical restriction of the hydrogel network and promote cartilage regeneration, several strategies have been explored including decreasing the polymer concentration to reduce the cross-linking density and increasing the pore size of hydrogels,<sup>10</sup> increasing the cell densities (up to 60 million per mL), culturing samples for longer durations (up to 8 weeks),<sup>11</sup> or decreasing the construct thickness.<sup>12</sup> Second, cartilage is a load-bearing tissue and upon implantation into the cartilage defect, hydrogels are subject to mechanical challenges including shear force and compressive loading, which can cause displacement or failure of the implanted construct.<sup>13</sup> Third, the compressive moduli of tissue-engineered cartilage using conventional hydrogels are often in the range of ~10–90 kPa,<sup>3,8,9,14–16</sup> which are an order of magnitude lower than those of native articular cartilage.<sup>17–19</sup> A few studies showed mechanical moduli comparable to those of native cartilage, but they require either dynamic hydrostatic loading and/or long-term culture (>8 weeks).<sup>20,21</sup> Although there are scaffolds with higher mechanical strength, such as collagen sponges, ceramics, and polyester based scaffolds, they are noninjectable and do not support minimal invasive delivery.<sup>22,23</sup>

To overcome the limitations associated with conventional hydrogels, our lab recently reported a macroporous, microribbon ( $\mu$ RB)-based hydrogel platform using gelatin (GEL) and polyethylene glycol (PEG).<sup>24,25</sup> Unlike conventional hydrogels, these  $\mu$ RB-based hydrogels are formed through a two-step cross-linking process, which renders the resulting scaffolds capable of absorbing shock and maintaining structural integrity upon cyclic compression. Furthermore,  $\mu$ RB-based hydrogels are macroporous and

support homogeneous cell encapsulation.<sup>24,25</sup> Compared to conventional GEL hydrogels, macroporous GEL  $\mu$ RB hydrogels significantly accelerated cartilage deposition by mesenchymal stem cells (MSCs) in three dimension (3D), resulting in an over 20-fold increase in the compressive modulus to ~220 kPa after only 3 weeks. In contrast, only minimal increases in compressive modulus were observed in MSC-seeded conventional GEL hydrogel controls.<sup>15</sup>

Whereas our previous report validated the advantage of macroporous GEL  $\mu$ RB hydrogels over conventional hydrogels for accelerating MSC-based cartilage regeneration, only GEL has been tested. How varying the  $\mu$ RB composition impacts MSC-based cartilage regeneration remains unknown. Chondroitin sulfate (CS) and hyaluronic acid (HA) are major glycosaminoglycans (GAGs) in the extracellular matrix (ECM) of articular cartilage. CS and HA stimulate chondrocyte metabolism, leading to increased cell proliferation, collagen production, and proteoglycan synthesis.<sup>26–28</sup> In addition, CS and HA hydrogels have shown efficacy for supporting MSC-based cartilage formation both *in vitro* and *in vivo*.<sup>5–9</sup> Our previous method for fabricating GEL  $\mu$ RBs uses dimethyl sulfoxide (DMSO) as the solvent, but CS and HA are only soluble in aqueous solvents. As such, there remains a need to develop a novel method that allows fabricating  $\mu$ RBs from polymers that are aqueous-soluble. Furthermore, while the compressive modulus of  $\mu$ RB-based engineered cartilage approached the compressive modulus of native articular cartilage, there remains a need to further increase the mechanical strength of engineered cartilage to match that of the native cartilage.

Compared to using single polymer composition-based hydrogels, mixed polymer composition hydrogels have been shown to further enhance stem cell differentiation toward cartilage,<sup>6,29–33</sup> bone,<sup>34</sup> and muscle lineages.<sup>35</sup> In conventional hydrogels and interpenetrating network hydrogels, each encapsulated cell senses mixed polymer compositions simultaneously as the entire polymer network is a homogeneous mixture of polymers.<sup>36</sup> However, in the  $\mu$ RB platform, each polymer is first cross-linked into a micron-sized  $\mu$ RB building block before mixing. Given that the width of individual  $\mu$ RBs (~100  $\mu$ m) is larger than individual cells, each cell only attaches and interacts with one  $\mu$ RB composition when encapsulated in mixed  $\mu$ RB scaffolds. As such, if MSCs were to be encapsulated in mixed  $\mu$ RB hydrogels composed of two different  $\mu$ RB compositions, it would result in two different cell populations coencapsulated in 3D. Whereas conventional hydrogels with mixed polymer compositions only allow modulation of cell–matrix interactions, mixed  $\mu$ RB scaffolds also enable modulation of cell fates through cell–cell interactions *via* paracrine signal exchange between two cell populations that are attached to two different  $\mu$ RB building blocks. The potential of harnessing mixed  $\mu$ RB scaffolds to enhance cartilage regeneration by MSCs has never been investigated before.

We hypothesize that tuning the  $\mu$ RB composition will modulate the speed and amount of cartilage deposition by MSCs in 3D, and mixing  $\mu$ RB compositions may further enhance MSC-based cartilage regeneration *via* paracrine signal exchange between cell populations attached to different  $\mu$ RB compositions. To test our hypotheses, we first developed a novel method that allows fabrication of  $\mu$ RBs from four different polymer compositions

(GEL, CS, HA, and PEG). Human MSCs were first encapsulated in scaffolds made of single composition  $\mu$ RBs and subsequently encapsulated in scaffolds made of mixed  $\mu$ RB compositions (1:1 ratio). To validate that the synergistic MSC-based cartilage production in the mixed  $\mu$ RBs is driven by paracrine signal exchange, conditioned media from MSCs seeded within single composition PEG or CS  $\mu$ RB scaffolds were exchanged in a dose-dependent manner. Finally, we further varied the ratio of PEG and CS  $\mu$ RBs in mixed  $\mu$ RB scaffolds to determine the optimal ratio of mixed  $\mu$ RBs for supporting MSC-based cartilage formation. All experiments were conducted in chondrogenic medium supplemented with transforming growth factor (TGF) $\beta$ -3 for 21 days. Outcomes were analyzed using scanning electron microscopy, mechanical testing, biochemical assays, histology, and immunofluorescence staining.

## 2. MATERIALS AND METHODS

### 2.1. Fabrication of Methacrylated $\mu$ RBs.

GEL  $\mu$ RBs were fabricated as previously reported.<sup>24</sup> Briefly, GEL type A was dissolved in DMSO at 19% w/v and wet spun into ethanol at 5 mL h<sup>-1</sup>. The  $\mu$ RBs were then methacrylated to enable photo-cross-linking and internally cross-linked using glutaraldehyde to fix their ribbon shape. HA (sodium hyaluronate, 40 kDa, Lifecore Biomedical) and CS (CS sodium salt from bovine cartilage, Sigma-Aldrich) precursors used for the fabrication of the  $\mu$ RBs were modified before spinning by reacting with *N*-(2-aminoethyl)acrylamide in 2-morpholinoethanesulfonic acid (MES) buffer and catalyzed by *N*-(3-dimethylaminopropyl)-*N'*-ethylcarbodiimide hydrochloride and acrylamide (Am) groups. The eight-arm 10 kDa PEG (JenKem Technology) precursor was modified with Am and maleimide by reacting eight-arm-PEG succinimidyl carbonate with *N*-(2-aminoethyl) acrylamide and *N*-(2-aminoethyl)-maleimide in dimethylformamide. The Am to maleimide ratio was controlled to be 3:1. To allow cell adhesion, the precursors were incorporated with 2.5 mM Cys-Arg-Gly-Asp-Ser (CRGDS). These precursors were then fabricated into  $\mu$ RBs using wet spinning, a process that was modified from what we reported previously.<sup>24,25</sup> Specifically, aqueous solutions of HA-Am and CS-Am (7.5% w/v) were injected into a propanol bath through a G31 needle at 0.5 mL h<sup>-1</sup>, and water extraction by propanol resulted in  $\mu$ RB-shaped fibers. GAG (HA and CS) precursors are not soluble in propanol; so the solid  $\mu$ RBs were left behind after water extraction by 2-propanol. The solid  $\mu$ RBs were collected and fixed by dithiothreitol (DTT) (~3% of the GAG molar repeats) in 2-propanol. Because PEG is slightly soluble in propanol, aqueous PEG solutions were fixed *in situ* during wet spinning. Precursor PEG solution was injected into a 2-propanol bath containing 0.3% DTT. Maleimide was used for intra-cross-linking, which reacts with DTT instantly during the spinning, leaving only Am groups on the formed PEG  $\mu$ RBs for inter-cross-linking. After internal fixation, all  $\mu$ RBs were washed six times in phosphate-buffered saline (PBS), snap-frozen, and lyophilized.

### 2.2. Scanning Electron Microscopy.

The morphology of hydrated  $\mu$ RB scaffolds was assessed using a Hitachi S-3400N variable pressure scanning electron microscope (SEM). The scaffolds were immersed in deionized (DI) water, loaded into the chamber, and gradually cooled from room temperature to -25 °C

as the chamber pressure decreased from 1 atm to 50 Pa, following a  $P/T$  curve during which water remains a liquid. The samples were imaged under electron beam intensity at 15 kV at a working distance around 12 mm.

### 2.3. Cell Encapsulation in 3D $\mu$ RB-Based Scaffolds.

Freeze-dried  $\mu$ RBs were rehydrated in PBS containing 0.1% lithium phenyl-2,4,6-trimethylbenzoylphosphinate, a commonly used photoinitiator,<sup>24,37</sup> for a final  $\mu$ RB density of 7.5% (w/v). Mixed  $\mu$ RB scaffolds were made by physically mixing different weight ratios of individual  $\mu$ RBs. The two  $\mu$ RB compositions were homogeneously mixed when hydrated. Human MSCs (Lonza, passage 6) were mixed with the rehydrated  $\mu$ RB paste to reach a density of 10 M mL<sup>-1</sup> and then photo-cross-linked into a 2 mm thick cell-laden hydrogel sheet by placing between two glass slides 2 mm apart and exposing to ultraviolet light (365 nm, 4 mW cm<sup>-2</sup>, 5 min). Cylindrical samples (4 mm diameter) were punched from the hydrogel sheet and transferred to 24-well plates for further culture. All samples were cultured for 21 days in chondrogenic medium with 10 ng mL<sup>-1</sup> TGF- $\beta$ 3 (PeproTech) as detailed previously<sup>38</sup> before analysis for cartilage production. On day 1, cell viability was assessed using a LIVE/DEAD Viability Kit (Thermo Fisher) as previously reported.<sup>15</sup>

### 2.4. Mechanical Testing.

To assess the ability of scaffolds to maintain structural integrity upon cyclic mechanical loading, cyclic compression and shear testing were performed on  $\mu$ RB scaffolds fabricated from single compositions (GEL, CS, HA, and PEG). For cyclic compression tests, samples were compressed at a rate of 1% strain s<sup>-1</sup> to a maximum strain of 30% for 10 cycles. Shear testing was performed using an ARES-G2 (TA Instruments) rheometer, with frequency sweeps at 10% strain coupled with a frequency change from 0.1 to 10 rad s<sup>-1</sup>. Cyclic shearing testing was conducted using 100% strain and a frequency of 1 Hz for 100 cycles. Unconfined compression tests were conducted using an Instron 5944 material testing system (Instron Corporation) fitted with a 10 N load cell (Interface, Inc.). To reduce friction, a polytetrafluoroethylene lined, custom-made aluminum compression plate was in contact with the sample. The sample diameter and thickness were measured before placing the sample in PBS. A 10 mN preload was added to each sample before compressing the sample at a rate of 1% strain s<sup>-1</sup>. The compressive moduli were determined from 10 to 20% of linear fit curve from the stress *versus* strain plot. The stiffness of individual  $\mu$ RBs was measured using atomic force microscopy (Park System NX10). Individual  $\mu$ RBs were attached to the glass cover slides and immersed in PBS. They were then indented with a colloidal cantilever (CP-PNP-SiO, NanoAndMore) with a force constant of 0.08 N m<sup>-1</sup> at an indentation speed of 1  $\mu$ m s<sup>-1</sup>. Young's modulus was calculated by fitting the force-indentation profile (200 pN to 2 nN) to a Hertzian model.

### 2.5. Biochemical Analyses.

On day 21, the scaffolds were harvested and measured for wet weight. They were then lyophilized and measured for dry weight. Swelling ratio was calculated as wet weight/dry weight of day 21 constructs. Each lyophilized sample was then digested in 500  $\mu$ L of papainase solution (Worthington Biochemical) for 16 h at 60 °C. Once digested, the supernatant from each sample was used for the DNA, sGAG, and collagen content assays,

as previously described.<sup>39,40</sup> DNA content was measured using the Quant-iT Picogreen dsDNA Assay Kit (Molecular Probes) and Lambda phage DNA as the standard. Fold proliferation was calculated as day 21 DNA content/day 1 DNA content. sGAG content was quantified using the 1,9-dimethylmethylene blue dye-binding assay with shark CS (Sigma-Aldrich) as the standard. Collagen content was measured using the Ehrlich's reaction assay for hydroxyproline. Briefly, samples were acid hydrolyzed and reacted with *p*-dimethylaminobenzaldehyde and chloramine T (Sigma). Total collagen content was estimated assuming 1:7.46 hydroxyproline: collagen mass ratio.

## 2.6. Histological Analyses.

On day 21, scaffolds were fixed in 4% paraformaldehyde (Sigma-Aldrich) for 1 h on an orbital shaker. Samples were then embedded in O.C.T. (Tissue Tek) overnight and snap frozen the following day. To visualize collagen and sGAG amount and distribution, Masson's trichrome staining (Thermo Scientific) and Safranin-O counterstained with fast green were performed, respectively. For immunostaining, the sections were incubated for 15 min at 37 °C for enzymatic antigen retrieval, for 1 h in blocking buffer containing 2% goat serum and 3% bovine serum albumin (BSA), and overnight at 4 °C in primary antibody solutions. Rabbit anti-human Col I, Col II, and Col X primary antibodies (Abcam) were diluted 1:100 and added to sample sections separately. The following day, the secondary antibody (Alexa Fluor 488 goat anti-rabbit) was diluted 1:200 with Hoechst (4  $\mu\text{g mL}^{-1}$ ). Sections were incubated with the secondary antibody solution for 1 h at room temperature. Samples were mounted in vectashield (Vector Laboratories) and imaged using a Zeiss fluorescence microscope.

## 2.7. Gene Expression.

Gene expression levels of mechanosensing (RhoA, ROCKI, and ROCKII) and cartilage-specific genes (collagen II, Aggrecan, Sox9) were analyzed on day 7. To extract total RNA,  $\mu\text{RB}$  samples were digested in TRIzol (Life Technologies), and RNA was precipitated using RNeasy Mini Kit columns (Qiagen). cDNA was synthesized from the extracted RNA using SuperScript III First-Strand Synthesis kit (Life Technologies). Real time polymerase chain reaction (RT-PCR) was performed using Power SYBR Green PCR Master Mix (Applied Biosystems, Life Technologies). RT-PCR primers are listed in Table S1. Relative expression levels of chondrogenic genes were determined by the Ct method. Chondrogenic gene expressions were first normalized to an endogenous housekeeping gene (hGAPDH) followed by a second normalization to the expression level measured in MSCs cultured in two dimension on tissue culture plastic on day 1.

## 2.8. BSA Diffusion Assay.

To characterize the diffusion throughout individual composition  $\mu\text{RB}$  scaffolds, we encapsulated 200  $\mu\text{L}$  of BSA into the  $\mu\text{RB}$  scaffolds, and the total percent of its release was measured over 48 h, using the methods previously described.<sup>41</sup>



## 2.9. Interaction Index Calculation.

Interaction indices provide a measure of interaction synergy for biochemical and mechanical analyses of the mixed  $\mu$ RB scaffolds. The calculated index is defined as the ratio of the experimental value over the expected value of a particular assay. An interaction index <1 indicates negative synergy, 1 indicates no synergy, and >1 indicates positive synergy. Interaction index for sGAG in the PEG–CS  $\mu$ RB scaffold

$$\frac{(sGAG_{\text{PEG-CS}})}{0.5(sGAG_{\text{PEG}}) + 0.5(sGAG_{\text{CS}})}$$

## 2.10. Confocal Imaging of Mixed $\mu$ RB Scaffolds.

Fluorescently labeled GEL and CS  $\mu$ RBs were used for confocal microscopy of mixed  $\mu$ RB scaffolds. GEL  $\mu$ RBs were mixed with 5  $\mu$ g/mL solution of Alexa Fluor 700 NHS ester, and CS  $\mu$ RBs were labeled with 5  $\mu$ g/mL solution of Alexa Fluor 488 NHS ester. MSCs were labeled with CellTracker CM-Dil dye (Thermo Fisher) as per the manufacturer's instructions. MSCs were encapsulated as above and imaged after 24 h of culture in the chondrogenic medium. A Leica SP8 microscope (Buffalo Grove, IL) was used to take the images.

## 2.11. Conditioned Medium Exchange Experiment.

To examine the effects of soluble factor exchange on MSC-based cartilage deposition in  $\mu$ RB scaffolds, conditioned medium from MSC-laden PEG or CS scaffolds was collected every other day, concentrated, and added to MSC-laden CS and PEG scaffolds, respectively. Every 2 days, the conditioned medium was collected and filter centrifuged to retain medium components that were >3 kDa (NMWL 3 kDa, Millipore Sigma). To examine the dose effect of soluble factors, we used concentrated conditioned medium ranging from 1 $\times$  to 10 $\times$ . A 10 $\times$  group meant that the conditioned medium from 10 MSC-seeded PEG  $\mu$ RB scaffolds was concentrated and added to one MSC-seeded CS  $\mu$ RB scaffold. The final volume of the conditioned medium added to each  $\mu$ RB scaffold, regardless of the initial starting volume, was 200  $\mu$ L. For example, for the 1 $\times$  group, the conditioned medium from one cell-seeded scaffold (1.5 mL) was concentrated to 200  $\mu$ L. For the 10 $\times$  group, the conditioned medium from 10 cell-seeded scaffolds (15 mL) was concentrated to 200  $\mu$ L. The concentrated conditioned medium at various dosages was then mixed with the fresh chondrogenic medium (1.3 mL) before adding to each cell-seeded scaffold.

## 2.12. Statistical Analysis.

All data are presented as mean  $\pm$  standard deviation (SD) (n = 3/group). GraphPad Prism (GraphPad Software) was used to perform a one-way analysis of variance followed by Tukey's multiple comparison test. Data are mean  $\pm$  SD for n = 3 samples. \*p < 0.05; \*\*p < 0.001.

### 3. RESULTS AND DISCUSSION

#### 3.1. Fabrication and Characterization of $\mu$ RBs with Tunable Compositions.

Our previous method of fabricating GEL  $\mu$ RBs used DMSO as the solvent and requires the solution to be highly viscous.<sup>24</sup> This is not suitable for CS, HA, or PEG, which are only soluble in aqueous solutions. As such, we first developed a new protocol to enable fabrication of  $\mu$ RBs from any aqueous soluble polymer, which we used to create CS, HA, and PEG  $\mu$ RBs. Briefly, CS and HA precursors were modified with Am, dissolved in DI water, and mixed with the cell adhesion peptide, CRGDS. The mixtures were wet-spun into an antisolvent propanol bath to obtain the  $\mu$ RB shape. The as-formed  $\mu$ RBs were subsequently transferred into a DTT solution to fix the  $\mu$ RB shape *via* reaction between DTT and Am. The remaining unreacted Am groups were used later for inter-cross-linking among  $\mu$ RBs *via* radical addition upon mixing with a photoinitiator to form 3D macroporous scaffolds. PEG was modified with maleimide to allow incorporation of CRGDS and was instantly cross-linked into  $\mu$ RB shape when wet-spun into a propanol bath containing DTT. PEG was also modified with Am groups, which allow inter-cross-linking among PEG  $\mu$ RBs or with other  $\mu$ RB compositions to form 3D macroporous scaffolds *via* radical addition upon mixing with a photoinitiator (Figure 1A).

Scanning electron microscopy confirmed successful formation of  $\mu$ RB building blocks from all four polymers with widths  $\sim$ 100–150  $\mu$ m, which subsequently inter-cross-linked to form macroporous 3D scaffolds (Figure 1B). Live/dead staining of the midsection of the scaffolds confirmed homogenous cell distribution in all groups after encapsulation, with comparable levels of high cell viability. In conventional hydrogels, the encapsulated cells often remain round because of physical restriction of the nanoporous hydrogel network.<sup>15</sup> In contrast to conventional hydrogels, in which encapsulated MSCs are rounded,<sup>15,38</sup> human MSCs showed adhesion and extensive cell spreading throughout the  $\mu$ RB scaffolds after just 24 h of culture (Figure 1C).

Given the importance of the weight-bearing property of articular cartilage, scaffolds for repairing cartilage defects need to maintain structural integrity when subject to cyclic loading before any new tissue is deposited. To assess the ability of the  $\mu$ RB scaffolds to survive such a challenge, we performed cyclic compression and oscillation tests. For cyclic compression testing, all  $\mu$ RB scaffolds were subject to 0–30% strain for 10 cycles. Natural ECM-derived  $\mu$ RB scaffolds (GEL, CS, and HA) exhibited great ability to maintain structural integrity upon cyclic compression loading (Figure 1D). By the end of 10 cycles of loading, GEL, CS, and HA retained 100, 93, and 76% of their original compressive moduli, respectively (Figure S1A). PEG  $\mu$ RB scaffolds appeared to lose partial integrity, retaining only 62% of its original compressive moduli (Figures 1D and S1A). For cyclic oscillation tests, all  $\mu$ RB scaffolds were subject to 100 cycles of oscillation up to 100% strain. A similar trend was observed, with natural ECM-derived  $\mu$ RB scaffolds (GEL, CS, and HA) exhibiting higher stability and the ability to withstand comparable maximum stresses at cycle 100 compared to cycle 1. In contrast, by cycle 100, PEG  $\mu$ RB scaffolds could only withstand  $\sim$ 40% of the maximum stress from the first cycle (Figures 1E and S1B). Together, our results validate that ECM-based  $\mu$ RB scaffolds can maintain their structure in a cyclic loading



environment, making them advantageous over conventional hydrogels which typically have a low fatigue resistance.

### 3.2. Speed and Amount of Neocartilage Formation by MSCs Depend on $\mu$ RB Composition.

We first evaluated the effect of varying  $\mu$ RB compositions on MSC-based cartilage formation using single-composition  $\mu$ RB scaffolds. After 21 days of culture in the chondrogenic medium, GEL  $\mu$ RB scaffolds resulted in ~3-fold cell proliferation (Figure 2A), whereas the cell number remained mostly unchanged in other  $\mu$ RB compositions. Overall,  $\mu$ RB scaffolds enhance cell proliferation compared to conventional hydrogels, which generally lead to a slight decrease in the cell number throughout *in vitro* chondrogenesis.<sup>42</sup> Similar to the trend observed with cell proliferation, GEL  $\mu$ RB scaffolds resulted in the highest amount of sGAG deposition by hMSCs, followed by HA and CS  $\mu$ RB scaffolds. PEG  $\mu$ RBs led to the lowest sGAG deposition (Figure 2B). The effect of varying  $\mu$ RB composition on total collagen deposition followed the same trend as sGAG (Figure 2C). Given the presence of collagen in GEL  $\mu$ RBs and the presence of sulfated GAGs in CS  $\mu$ RBs, we also performed quantification of acellular scaffolds on day 21 as controls (Figure 2A,B). Even when accounting for differences in the starting levels of sGAG and collagen from the hydrogels themselves, GEL  $\mu$ RBs still outperformed the rest.

Compressive properties of engineered cartilage produced by MSCs encapsulated in various  $\mu$ RB compositions followed the same trend as the results of biochemical assays and histology (Figure 2D). After only 3 weeks of culture, MSCs encapsulated in the ECM-based  $\mu$ RB scaffolds resulted in neotissue with compressive moduli ranging from 150 kPa to above 250 kPa. For GEL  $\mu$ RBs, this is an ~30-fold increase in compressive moduli within a short time (Figures 2D and S2) and approaches the lower limit of compressive modulus of native articular cartilage.<sup>17–19</sup> The rapid increase in compressive stiffness of engineered cartilage in our  $\mu$ RB scaffolds is a major improvement compared to conventional hydrogels, which generally produce cartilage with slow increases in compressive moduli that are limited to only ~10–90 kPa even after months of culture *in vitro*.<sup>3,8,9,14–16</sup> Although some previous strategies have demonstrated the ability to produce cartilage with comparable compressive moduli, they require much longer culture time (that is, 8 weeks *vs* 3 weeks in our study), much higher cell densities (60 million per mL *vs* 10 million per mL in our study), or thinner constructs (0.78 mm *vs* 2 mm in our study).<sup>11,12</sup> We speculate that one reason  $\mu$ RB scaffolds resulted in cartilage with substantially enhanced mechanical property is its demonstrated efficacy to promote interconnectivity among the newly deposited matrix. Because of inherent interconnected macroporosity in  $\mu$ RB scaffolds, cells within all ECM  $\mu$ RB scaffolds produced highly interconnected sGAG (Figures 3A and S3A) and collagen (Figures 3B and S3B) deposition. In these images, there is a clear distinction in the appearance of sGAG and collagen staining from the  $\mu$ RB scaffold and from cellular deposition. GEL  $\mu$ RBs appear as dark blue in trichrome, and CS  $\mu$ RBs appear as dark red in Safranin-O. However, cell-deposited collagen appears as light blue and cell-deposited sGAG appears as light red. This is an important improvement in the distribution of newly deposited ECM compared to conventional hydrogels, in which the ECM deposition is often highly discrete and limited only to pericellular regions.<sup>3–9</sup> GEL  $\mu$ RBs supported the most robust

and interconnected distribution of sGAG and collagen. HA and CS  $\mu$ RBs resulted in an intermediate level of sGAG and collagen deposition, followed by PEG  $\mu$ RBs (Figures 3A,B and S3A,B). We also performed staining on acellular d21 scaffolds to account for sGAG (Figure S4A) and collagen (Figure S4B) present in the scaffold itself. When compared to the staining from acellular scaffolds, cellular scaffolds clearly showed that a majority of sGAG and collagen were deposited by encapsulated MSCs and filled up the macropores within the  $\mu$ RB scaffolds. Varying  $\mu$ RB composition also modulated the phenotype of the newly formed cartilaginous tissue. Among the four tested  $\mu$ RB compositions, GEL  $\mu$ RB led to the greatest amount of type II collagen (a marker for hyaline cartilage), minimal type X collagen (a marker for hypertrophic cartilage), and high type I collagen (a marker of fibroblastic cartilage) (Figure 3C–E).

Our findings that GEL  $\mu$ RBs outperformed GAG-based  $\mu$ RBs in enhancing MSC-based cartilage deposition in 3D was unexpected. GEL is a digested form of type I collagen, which is not a native cartilage ECM composition, as the articular cartilage matrix is composed of mostly type II collagen. In contrast, CS and HA are two major cartilage-ECM compositions and have been shown to support MSC-based cartilage formation when used as conventional hydrogels.<sup>5–9</sup> A previous study compared GEL and HA conventional hydrogels as 3D niche for supporting MSC chondrogenesis. Contrary to the trend we observed in  $\mu$ RB scaffolds, HA-based conventional hydrogels outperformed GEL hydrogels in supporting neocartilage deposition.<sup>29</sup> Physical properties of diffusion and swelling do not differ significantly between the  $\mu$ RB scaffolds (Figure S5); so they are not responsible for differences in MSC behavior. However, there are minimal differences in construct dimensions; so MSC contractility abilities could have led to some differences in the phenotype (Figure S6). Differences in charge, protein absorption, and growth factor interactions/sequestration also likely influence the chondrogenic behavior of the encapsulated MSCs. Together, these results suggest that MSCs respond to changes in biomaterial compositions in macroporous  $\mu$ RB scaffolds in unique ways, which cannot be predicted from conventional hydrogel results.

Varying the  $\mu$ RB composition can change the biochemical and mechanical cues simultaneously. The stiffness of the individual  $\mu$ RBs, which the cells directly sense as a substrate, was characterized using atomic force microscopy. Our results showed that stiffness of  $\mu$ RBs ranged between ~8 and 40 kPa, with GEL  $\mu$ RB as the softest and CS  $\mu$ RB as the stiffest (Figure S7A). Unlike GEL, CS and HA are highly negatively charged polymers and swell more in aqueous solution. To prevent excessive swelling, higher intra-cross-linking density was required for fabrication of CS and HA  $\mu$ RBs, therefore resulting in higher stiffness. Previous 2D studies have shown that mechanosensing correlates with the cell shape, with increased cell spreading leading to upregulated gene expressions of RhoA/ROCK.<sup>43</sup> Despite the differences in  $\mu$ RB stiffness, MSCs demonstrated comparable level of expressions of mechanosensing genes including RhoA, ROCKI, and ROCKII (Figure S7B–D). Likely due to the comparable level of extensive cell spreading observed in all  $\mu$ RB compositions (Figure 1C), MSCs on all  $\mu$ RB compositions sense the substrates in a similar manner. Together, these results suggest that changes in biochemical cues, not stiffness, were responsible for the differential amount of cartilage regeneration by MSCs encapsulated in different  $\mu$ RB compositions.

### 3.3. Mixed $\mu$ RB Scaffolds Induce High Synergy with Rapid and Robust Cartilage Formation.

Previous work using conventional hydrogels have shown the benefits of mixing GAGs into GEL or PEG hydrogels to improve cartilage production.<sup>6,29–33</sup> Given all  $\mu$ RB compositions are able to be inter-cross-linked with the same photoinitiator, they can be easily mixed to form composite scaffolds. We further assessed the effects of mixed  $\mu$ RBs on MSC-based cartilage formation by mixing GEL or PEG  $\mu$ RBs with GAG  $\mu$ RBs in a 1:1 ratio. Surprisingly, all mixed  $\mu$ RB scaffolds supported rapid and robust new cartilage deposition by MSCs as shown by cell proliferation, sGAG, and collagen production (Figure 4A–C). Mixed  $\mu$ RB scaffolds composed of 1:1 of GEL and CS  $\mu$ RBs led to the highest cell proliferation, the greatest amount of sGAG and collagen deposition, and the highest compressive modulus of  $553 \pm 120$  kPa (Figure 4). Compared with the total amount of matrix produced in the MSC-containing scaffolds, the sGAG and collagen background from acellular  $\mu$ RB scaffolds was much lower (Figure 4A,B). These results confirmed that most of the collagen and sGAG from cellular scaffolds were contributed by the newly formed cartilage rather than the background from scaffold compositions.

To quantify the synergy in mixed  $\mu$ RB scaffolds, we calculated the interaction index, which is the ratio of the experimental value from the mixed  $\mu$ RB group normalized to the combined value from 50% of each of the two  $\mu$ RB compositions when cultured as single composition scaffolds.<sup>44</sup> All interaction indices were greater than 1, indicating a positive synergistic interaction for proliferation (Figure 5A), sGAG deposition (Figure 5B), collagen deposition (Figure 5C), and compressive moduli (Figure 5D). The highest synergy was measured in the mixed  $\mu$ RB groups containing PEG. This is probably due to the fact that PEG  $\mu$ RB alone resulted in the lowest cartilage formation by MSCs in 3D (Figure 2), whereas adding GAG  $\mu$ RBs to PEG  $\mu$ RBs substantially enhanced cartilage formation.

Histological staining also showed the same trend as biochemical assays, with all mixed  $\mu$ RB groups resulting in intense and interconnected sGAG and collagen deposition (Figures 6A,B and S3C,D). Given GAG and GEL  $\mu$ RBs have background staining, we also performed staining of acellular scaffolds on day 21 as controls (Figure S4C,D). It is clear that  $\mu$ RB scaffolds were filled mostly with a cell-deposited cartilage matrix by MSCs by 3 weeks of culture. The leading group, GEL–CS, showed the most intense cartilage matrix sGAG, collagen, and collagen II production (Figures 6A–C and S3C,D). All mixed scaffolds resulted in a minimal expression of collagen type X (Figure 6D), suggesting minimal hypertrophic cartilage phenotype and similar baseline amounts of collagen type I (Figure 6E).

Although mixing polymer compositions has been reported to enhance cartilage formation by stem cells in conventional hydrogels, the degree of synergy is much less compared to the level of synergy observed in mixed  $\mu$ RB scaffolds.<sup>6,29–33</sup> Furthermore, the mechanism and extent of such synergy are very different in composite conventional hydrogels and composite  $\mu$ RB scaffolds. In conventional hydrogels, mixing polymer compositions results in a nanoscale mixture of both biochemical cues. Each individual cell interacts with multiple polymer compositions simultaneously. In contrast, each individual cell only attaches to one single  $\mu$ RB as the width of an individual  $\mu$ RB ( $\sim 100$ – $150$   $\mu$ m) is much larger than individual

cells.<sup>45</sup> As such, whether encapsulated in a single composition or mixed composition  $\mu$ RB scaffold, a majority of individual cells only attach, interact, and sense one  $\mu$ RB at a time (Figure S8). As shown by the quantitative gene expression, MSCs attached to different  $\mu$ RB compositions exhibit differential levels of chondrogenesis (Figure S9). Therefore, it is reasonable to speculate that there are two distinct cell populations within a mixed  $\mu$ RB scaffold. There is minimal direct cell–cell contact between cells on different  $\mu$ RBs, but the paracrine signals secreted by the cells attached to different  $\mu$ RBs can freely diffuse and exchange because of macroporosity in the  $\mu$ RB scaffolds. Given this unique feature of  $\mu$ RB scaffolds, we speculated that the enhanced synergy we observed in the mixed  $\mu$ RB scaffolds was driven by the exchange of soluble factors secreted by MSCs seeded on different  $\mu$ RBs.

### 3.4. Mixed $\mu$ RB-Induced Synergy Can Be Recapitulated by the Exchange of Conditioned Medium from MSCs Cultured in Individual $\mu$ RBs in a Dose-Dependent Manner.

To validate whether the cell-secreted soluble factor exchange was responsible for the synergized cartilage formation observed in the mixed  $\mu$ RBs, we performed a conditioned medium exchange study (Figure 7A). We chose PEG and CS  $\mu$ RBs as a model system because this combination resulted in the highest interaction indices for cartilage matrix production in mixed composition scaffolds (Figure 5B,C). Briefly, the conditioned medium from MSCs cultured in either PEG or CS  $\mu$ RB scaffolds alone was collected, concentrated, and added to MSCs encapsulated in the opposite  $\mu$ RB composition at various dosages. Indeed, the conditioned medium exchange increased cartilage deposition by MSCs in both the scaffolds in a dose-dependent manner, with the 5–10 $\times$  concentrated conditioned medium resulting in the greatest sGAG deposition. As a control, we also added 10 $\times$  concentrated conditioned medium from each  $\mu$ RB to itself (that is, CS to CS), which showed much less cartilage formation compared to the conditioned medium exchange treatment (PEG to CS and CS to PEG, 10 $\times$ ) (Figure 7B,C). This confirmed that the increase in cartilage production was not due to increased concentrations of autocrine factors or growth factors present in the concentrated medium itself but from cell-secreted paracrine factors.

Whereas synergy was observed in both the scaffolds, the increase in cartilage formation was much more substantial on adding the conditioned medium from PEG to CS  $\mu$ RBs (Figure 7B) than from CS to PEG  $\mu$ RBs (Figure 7C). These results suggest that the enhanced cartilage formation in the mixed  $\mu$ RB group is contributed more by the MSCs attached to CS  $\mu$ RBs. MSCs encapsulated in individual composition PEG  $\mu$ RB scaffolds and cultured in chondrogenic medium do not upregulate chondrogenic markers to the same extent as MSCs encapsulated in CS  $\mu$ RB scaffolds (Figure S9). This could indicate that MSCs attached to PEG  $\mu$ RBs remain in a more stemlike fate and catalyze more chondrogenically differentiated MSCs on CS  $\mu$ RBs to produce more ECM, as has been demonstrated in the coculture of stem cells catalyzing cartilage formation of neonatal chondrocytes.<sup>46</sup> Furthermore, although conditioned medium exchange induced synergy, the amount of final cartilage deposition induced by the conditioned medium exchange was less than what was observed in the mixed PEG–CS  $\mu$ RB scaffold (Figures 6A and S3C). This may be due to the dynamic cell–cell interactions in the mixed  $\mu$ RB scaffold, which were not present in the conditioned medium exchange model. Given MSCs underwent chondrogenesis during the culture period, the

paracrine signals they secreted likely changed and effected other MSCs in the mixed  $\mu$ RB scaffold in ways not fully recapitulated in the conditioned medium exchange model.

### 3.5. Varying the Ratio of Mixed $\mu$ RBs Allows Further Optimization of Cartilage Formation.

Given the extent of cartilage formation induced by the conditioned medium exchange is dose-dependent, we speculated that MSC-based cartilage deposition in  $\mu$ RB scaffolds could be further optimized by tuning the ratios of mixed  $\mu$ RBs. To test this, MSCs were encapsulated in mixed PEG-CS  $\mu$ RBs with increasing ratios of CS from 10 to 90%. PEG- or CS-only  $\mu$ RB scaffolds were included as controls. Mixed  $\mu$ RB scaffolds containing 50 or 75% CS resulted in the highest amount of collagen and sGAG deposition (Figure 8A,B) and the highest levels of collagen II (Figure 8C) accompanied by the lowest level of collagen X staining (Figure 8D). All groups resulted in similar amounts of collagen I (Figure 8E). Biochemical analyses confirmed the same trend, with 50 and 75% CS  $\mu$ RB leading to the highest cell proliferation, sGAG and collagen deposition, and compressive moduli (Figure 8F–I). Impressively, mixed  $\mu$ RB group containing 75% CS led to the highest compressive modulus ( $524 \pm 15$  kPa), comparable to that of native articular cartilage. Together, these results support the efficacy of optimizing cartilage formation by simply varying the ratios of mixed  $\mu$ RBs.

One limitation of using MSCs for articular cartilage tissue engineering is that bone marrow MSCs share many characteristics with fibroblasts, such as expression of high levels of collagen type I.<sup>47</sup> When encapsulated in conventional hydrogels with chondrogenic factors present, MSCs often result in cartilage with a high collagen I expression, indicative of the fibroblastic cartilage phenotype.<sup>5,48</sup> Our results demonstrated that MSCs also expressed high levels of collagen I in  $\mu$ RB scaffolds regardless of the composition (Figures 3E, 6E, and 8E). Future studies may use siRNA delivery or other gene-silencing techniques to reduce such undesirable fibrocartilage phenotype.

Future research will work to optimize construct properties for cartilage tissue engineering by exploring different ratios of GEL–CS  $\mu$ RB scaffolds. Additionally, despite creating constructs with robust sGAG and collagen deposition, the proportion of collagen: sGAG should better match the native cartilage to help achieve more biomimetic structure and function.

## 4. CONCLUSIONS

In summary, here we report a method that allows fabrication of natural ECM-derived and synthetic polymers into  $\mu$ RB structures as building blocks for forming 3D macroporous niches to accelerate MSC-based cartilage regeneration. These “Lego-like”  $\mu$ RB building blocks share the same inter-cross-linking chemistry and can be easily mixed in any ratio in a modular manner. Whereas conventional hydrogels with mixed polymer compositions only allow modulate cell–matrix interactions, mixed  $\mu$ RB-based scaffolds allow modulation of both cell–matrix and cell–cell interactions, leading to synergistic interactions among encapsulated MSCs and substantially accelerated cartilage regeneration. The leading mixed  $\mu$ RB formulation enabled fast restoration of cartilagemimicking compressive modulus after only 3 weeks of culture, which is 1 order of magnitude higher than what has been

achieved using conventional hydrogels. Using a conditioned medium exchange model, we further validated that such synergy can be recapitulated by paracrine signaling exchange between cells attached to different  $\mu$ RB compositions. The paracrine signal exchange can be directly tuned by varying the  $\mu$ RB ratio in the mixed  $\mu$ RB scaffolds, which allows further optimization of the speed of MSC-based cartilage regeneration. The results from the present study provide solid foundations for future studies to further validate the efficacy of mixed  $\mu$ RBs to enhance MSC-based cartilage regeneration using relevant animal models. It remains unclear what specific soluble factors are responsible for the induced synergy in cartilage deposition in mixed  $\mu$ RB scaffolds. We speculate such factors are multifactorial and change over time as the MSCs differentiate into chondrocytes. Future studies using gene microarrays or high-throughput analyses of protein profiles will likely be necessary to further elucidate the underlying complex mechanisms. Whereas this paper focuses on cartilage as a model tissue system, the concept of using mixed  $\mu$ RB-based scaffolds to induce synergy *via* modulating cell–cell paracrine signal exchange may be broadly applicable for enhancing stem cell regeneration for other tissue types.

## Supplementary Material

Refer to Web version on PubMed Central for supplementary material.

## ACKNOWLEDGMENTS

The authors would like to thank NIH R01DE024772, NIH R01AR074502, Stanford Coulter translational grant, Stanford SPARK program, and Stanford Bio-X Interdisciplinary initiative program for funding. C.G. would like to thank the Stanford Bio-X graduate fellowship for support. The authors would also like to thank Anthony Behn for technical assistance with mechanical testing.

## REFERENCES

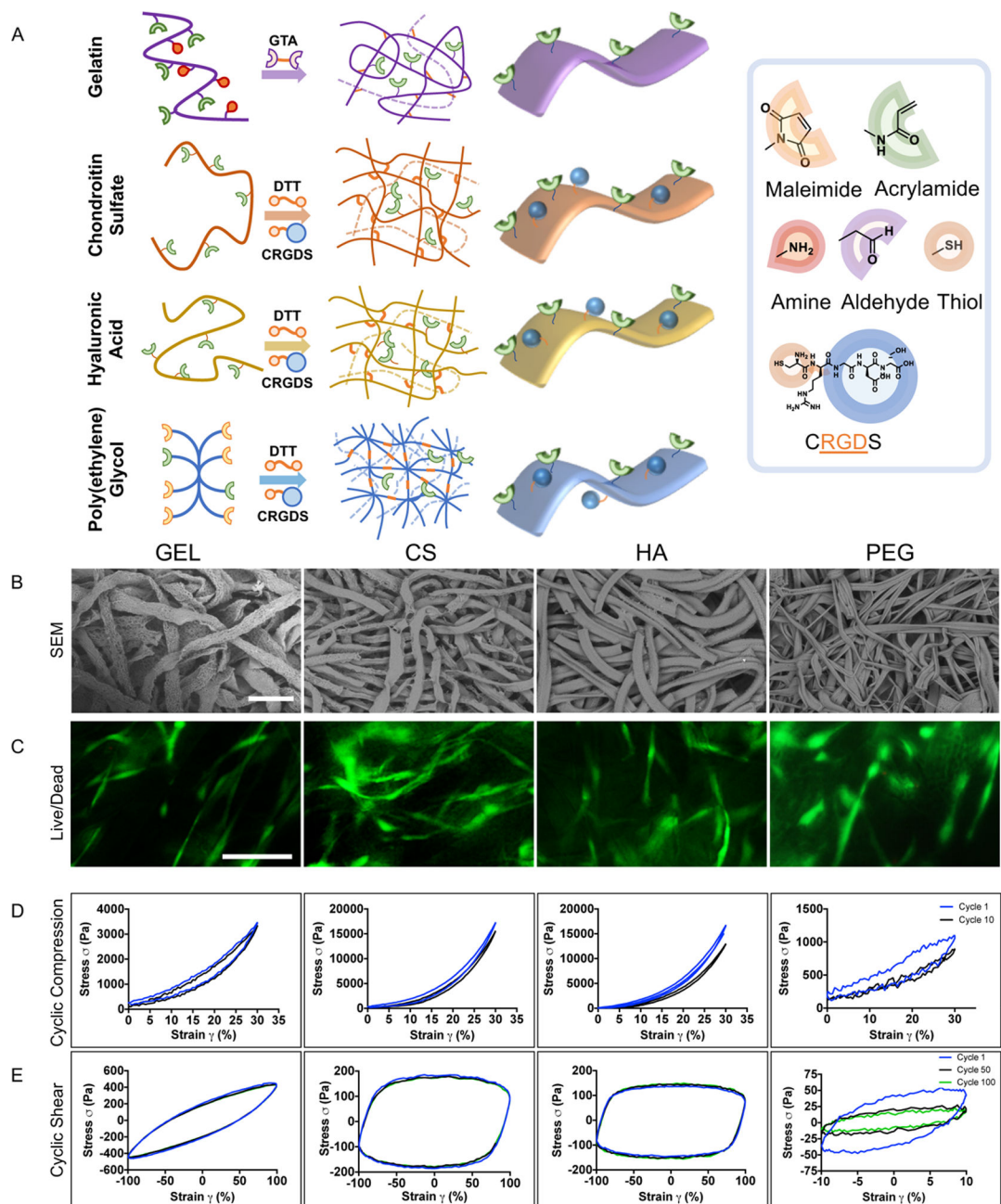
- (1). Zhu J; Marchant RE Design properties of hydrogel tissue engineering scaffolds. *Expert Rev. Med. Devices* 2011, 8, 607–626. [PubMed: 22026626]
- (2). Tan H; Marra KG Injectable, Biodegradable Hydrogels for Tissue Engineering Applications. *Materials* 2010, 3, 1746–1767.
- (3). Lin H; Cheng AW-M; Alexander PG; Beck AM; Tuan RS Cartilage tissue engineering application of injectable gelatin hydrogel with in situ visible-light-activated gelation capability in both air and aqueous solution. *Tissue Eng., Part A* 2014, 20, 2402–2411. [PubMed: 24575844]
- (4). Visser J; Gawlitta D; Benders KEM; Toma SMH; Pouran B; van Weeren PR; Dhert WJA; Malda J Endochondral bone formation in gelatin methacrylamide hydrogel with embedded cartilage-derived matrix particles. *Biomaterials* 2015, 37, 174–182. [PubMed: 25453948]
- (5). Chung C; Burdick JA Influence of three-dimensional hyaluronic acid microenvironments on mesenchymal stem cell chondrogenesis. *Tissue Eng., Part A* 2009, 15, 243–254.
- (6). Varghese S; Hwang NS; Canver AC; Theprungsirikul P; Lin DW; Elisseeff J Chondroitin sulfate based niches for chondrogenic differentiation of mesenchymal stem cells. *Matrix Biol.* 2008, 27, 12–21. [PubMed: 17689060]
- (7). Hwang NS; Varghese S; Li H; Elisseeff J Regulation of osteogenic and chondrogenic differentiation of mesenchymal stem cells in PEG-ECM hydrogels. *Cell Tissue Res.* 2011, 344, 499–509. [PubMed: 21503601]
- (8). Bian L; Guvendiren M; Mauck RL; Burdick JA Hydrogels that mimic developmentally relevant matrix and N-cadherin interactions enhance MSC chondrogenesis. *Proc. Natl. Acad. Sci. U.S.A.* 2013, 110, 10117–10122. [PubMed: 23733927]



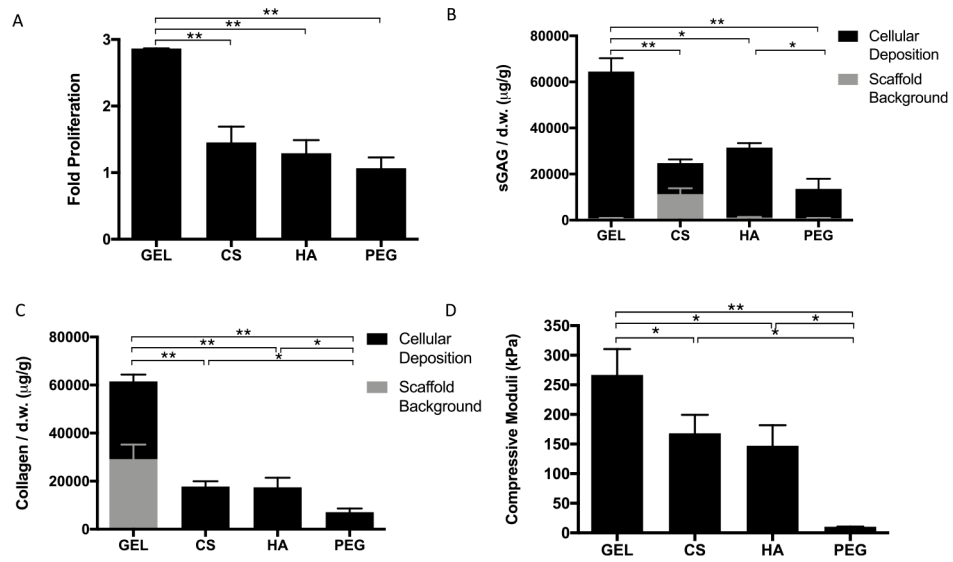
- (9). Bian L; Hou C; Tous E; Rai R; Mauck RL; Burdick JA The influence of hyaluronic acid hydrogel crosslinking density and macromolecular diffusivity on human MSC chondrogenesis and hypertrophy. *Biomaterials* 2013, 34, 413–421. [PubMed: 23084553]
- (10). Erickson IE; Huang AH; Sengupta S; Kestle S; Burdick JA; Mauck RL Macromer density influences mesenchymal stem cell chondrogenesis and maturation in photocrosslinked hyaluronic acid hydrogels. *Osteoarthr. Cartil.* 2009, 17, 1639–1648.
- (11). Erickson IE; Kestle SR; Zellars KH; Farrell MJ; Kim M; Burdick JA; Mauck RL High mesenchymal stem cell seeding densities in hyaluronic acid hydrogels produce engineered cartilage with native tissue properties. *Acta Biomater.* 2012, 8, 3027–3034. [PubMed: 22546516]
- (12). Bian L; Angione SL; Ng KW; Lima EG; Williams DY; Mao DQ; Ateshian GA; Hung CT Influence of decreasing nutrient path length on the development of engineered cartilage. *Osteoarthr. Cartil.* 2009, 17, 677–685.
- (13). DeKosky BJ; Dormer NH; Ingavle GC; Roatch CH; Lomakin J; Detamore MS; Gehrke SH Hierarchically designed agarose and poly(ethylene glycol) interpenetrating network hydrogels for cartilage tissue engineering. *Tissue Eng., Part C* 2010, 16, 1533–1542.
- (14). Chung C; Beecham M; Mauck RL; Burdick JA The influence of degradation characteristics of hyaluronic acid hydrogels on in vitro neocartilage formation by mesenchymal stem cells. *Biomaterials* 2009, 30, 4287–4296. [PubMed: 19464053]
- (15). Conrad B; Han LH; Yang F Gelatin-based microribbon hydrogels accelerate cartilage formation by mesenchymal stem cells in 3D. *Tissue Eng., Part A* 2018, 24, 1631–1640. [PubMed: 29926770]
- (16). Yao H; Xue J; Wang Q; Xie R; Li W; Liu S; Cai J; Qin D; Wang D-A; Ren L Glucosamine-modified polyethylene glycol hydrogel-mediated chondrogenic differentiation of human mesenchymal stem cells. *Mater. Sci. Eng., C* 2017, 79, 661–670.
- (17). Mow VC; Guo XE Mechano-electrochemical properties of articular cartilage: their inhomogeneities and anisotropies. *Annu. Rev. Biomed. Eng.* 2002, 4, 175–209. [PubMed: 12117756]
- (18). Jurvelin JS; Buschmann MD; Hunziker EB Optical and mechanical determination of Poisson's ratio of adult bovine humeral articular cartilage. *J. Biomech.* 1997, 30, 235–241. [PubMed: 9119822]
- (19). Little CJ; Bawolin NK; Chen X Mechanical properties of natural cartilage and tissue-engineered constructs. *Tissue Eng., Part B* 2011, 17, 213–227.
- (20). Erickson I Optimization and Translation of MSC-Based Hyaluronic Acid Hydrogels for Cartilage Repair. PhD Thesis, University of Pennsylvania, 2011.
- (21). Lima EG; Bian L; Ng KW; Mauck RL; Byers BA; Tuan RS; Ateshian GA; Hung CT The beneficial effect of delayed compressive loading on tissue-engineered cartilage constructs cultured with TGF-beta3. *Osteoarthritis and cartilage / OARS. Osteoarthr. Cartil.* 2007, 15, 1025–1033.
- (22). O'Brien FJ Biomaterials & scaffolds for tissue engineering. *Mater. Today* 2011, 14, 88–95.
- (23). Izadifar Z; Chen X; Kulyk W Strategic Design and Fabrication of Engineered Scaffolds for Articular Cartilage Repair. *J. Funct. Biomater.* 2012, 3, 799–838. [PubMed: 24955748]
- (24). Han L-H; Yu S; Wang T; Behn AW; Yang F Microribbon-Like Elastomers for Fabricating Macroporous and Highly Flexible Scaffolds that Support Cell Proliferation in 3D. *Adv. Funct. Mater.* 2013, 23, 346–358.
- (25). Han L-H; Tong X; Yang F Photo-crosslinkable PEG-based microribbons for forming 3D macroporous scaffolds with decoupled niche properties. *Adv. Mater.* 2014, 26, 1757–1762. [PubMed: 24347028]
- (26). Patti AM; Gabriele A; Vulcano A; Ramieri MT; Della Rocca C Effect of hyaluronic acid on human chondrocyte cell lines from articular cartilage. *Tissue Cell* 2001, 33, 294–300. [PubMed: 11469544]
- (27). Akmal M; Singh A; Anand A; Kesani A; Aslam N; Goodship A; Bentley G The effects of hyaluronic acid on articular chondrocytes. *J. Bone Jt. Surg. Br. Vol.* 2005, 87-B, 1143–1149.

- (28). Jerosch J Effects of Glucosamine and Chondroitin Sulfate on Cartilage Metabolism in OA: Outlook on Other Nutrient Partners Especially Omega-3 Fatty Acids. *Int. J. Rheumatol.* 2011, 2011, 969012. [PubMed: 21826146]
- (29). Moulisová V; Poveda-Reyes S; Sanmartín-Masiá E; Quintanilla-Sierra L; Salmerón-Sánchez M; Gallego Ferrer G Hybrid Protein-Glycosaminoglycan Hydrogels Promote Chondrogenic Stem Cell Differentiation. *ACS Omega* 2017, 2, 7609–7620. [PubMed: 29214232]
- (30). Wang T; Lai JH; Han L-H; Tong X; Yang F Chondrogenic differentiation of adipose-derived stromal cells in combinatorial hydrogels containing cartilage matrix proteins with decoupled mechanical stiffness. *Tissue Eng., Part A* 2014, 20, 2131–2139. [PubMed: 24707837]
- (31). Nguyen LH; Kudva AK; Guckert NL; Linse KD; Roy K Unique biomaterial compositions direct bone marrow stem cells into specific chondrocytic phenotypes corresponding to the various zones of articular cartilage. *Biomaterials* 2011, 32, 1327–1338. [PubMed: 21067807]
- (32). Steinmetz NJ; Bryant SJ Chondroitin sulfate and dynamic loading alter chondrogenesis of human MSCs in PEG hydrogels. *Biotechnol. Bioeng.* 2012, 109, 2671–2682. [PubMed: 22511184]
- (33). Levett PA; Melchels FPW; Schrobback K; Hutmacher DW; Malda J; Klein TJ A biomimetic extracellular matrix for cartilage tissue engineering centered on photocurable gelatin, hyaluronic acid and chondroitin sulfate. *Acta Biomaterialia* 2014, 10, 214–223. [PubMed: 24140603]
- (34). Wang L; Stegemann JP Thermogelling chitosan and collagen composite hydrogels initiated with beta-glycerophosphate for bone tissue engineering. *Biomaterials* 2010, 31, 3976–3985. [PubMed: 20170955]
- (35). Ding K; Yang Z; Zhang Y-L; Xu J-Z Injectable thermosensitive chitosan/beta-glycerophosphate/collagen hydrogel maintains the plasticity of skeletal muscle satellite cells and supports their in vivo viability. *Cell Biol. Int.* 2013, 37, 977–987. [PubMed: 23620126]
- (36). Dragan ES Design and applications of interpenetrating polymer network hydrogels. A review. *Chem. Eng. J.* 2014, 243, 572–590.
- (37). Fairbanks BD; Schwartz MP; Bowman CN; Anseth KS Photoinitiated polymerization of PEG-diacrylate with lithium phenyl-2,4,6-trimethylbenzoylphosphinate: polymerization rate and cytocompatibility. *Biomaterials* 2009, 30, 6702–6707. [PubMed: 19783300]
- (38). Wang T; Yang F, A comparative study of chondroitin sulfate and heparan sulfate for directing three-dimensional chondrogenesis of mesenchymal stem cells. *Stem Cell Res. Ther.* 2017, 8. DOI: 10.1186/s13287-017-0728-6
- (39). Neuman RE; Logan MA The determination of hydroxyproline. *J. Biol. Chem.* 1950, 184, 299–306. [PubMed: 15421999]
- (40). Wang T; Lai JH; Yang F Effects of Hydrogel Stiffness and Extracellular Compositions on Modulating Cartilage Regeneration by Mixed Populations of Stem Cells and Chondrocytes In Vivo. *Tissue Eng., Part A* 2016, 22, 1348–1356. [PubMed: 27676200]
- (41). Lee S; Tong X; Yang F Effects of the poly(ethylene glycol) hydrogel crosslinking mechanism on protein release. *Biomater. Sci.* 2016, 4, 405–411. [PubMed: 26539660]
- (42). Sharma B; Fermanian S; Gibson M; Unterman S; Herzka DA; Cascio B; Coburn J; Hui AY; Marcus N; Gold GE; Elisseeff JH Human cartilage repair with a photoreactive adhesive-hydrogel composite. *Sci. Transl. Med.* 2013, 5, 167ra6.
- (43). Bhadriraju K; Yang M; Alom Ruiz S; Pirone D; Tan J; Chen CS Activation of ROCK by RhoA is regulated by cell adhesion, shape, and cytoskeletal tension. *Exp. Cell Res.* 2007, 313, 3616–3623. [PubMed: 17673200]
- (44). Tallarida RJ The interaction index: a measure of drug synergism. *Pain* 2002, 98, 163–168. [PubMed: 12098628]
- (45). Ge J; Guo L; Wang S; Zhang Y; Cai T; Zhao RCH; Wu Y The size of mesenchymal stem cells is a significant cause of vascular obstructions and stroke. *Stem Cell Rev. Rep.* 2014, 10, 295–303. [PubMed: 24390934]
- (46). Lai JH; Kajiyama G; Smith RL; Maloney W; Yang F Stem cells catalyze cartilage formation by neonatal articular chondrocytes in 3D biomimetic hydrogels. *Sci. Rep.* 2013, 3, 3553. [PubMed: 24352100]

- (47). Denu RA; Nemcek S; Bloom DD; Goodrich AD; Kim J; Mosher DF; Hematti P Fibroblasts and Mesenchymal Stromal/Stem Cells Are Phenotypically Indistinguishable. *Acta Haematol.* 2016, 136, 85–97. [PubMed: 27188909]
- (48). Zheng L; Fan HS; Sun J; Chen XN; Wang G; Zhang L; Fan YJ; Zhang XD Chondrogenic differentiation of mesenchymal stem cells induced by collagen-based hydrogel: an in vivo study. *J. Biomed. Mater. Res., Part A* 2010, 93, 783–792.

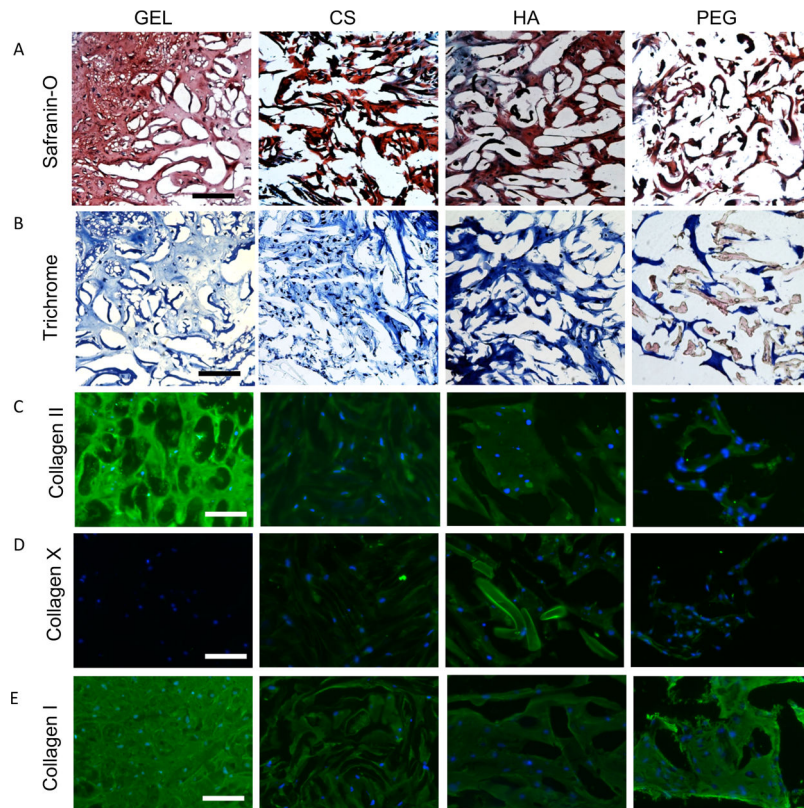
**Figure 1.**

Fabrication and characterization of  $\mu$ RB-based hydrogels. (A) Schematic for fabricating  $\mu$ RBs from a variety of natural and synthetic polymers. (B) SEM images of cross-linked  $\mu$ RB-based hydrogels, demonstrating macroporosity. (C) Live/dead staining on day 1 of MSC encapsulation. (D) Cyclic compression testing. (E) Cyclic shear testing. Scale bars: (B) 250 and (C) 100  $\mu$ m.



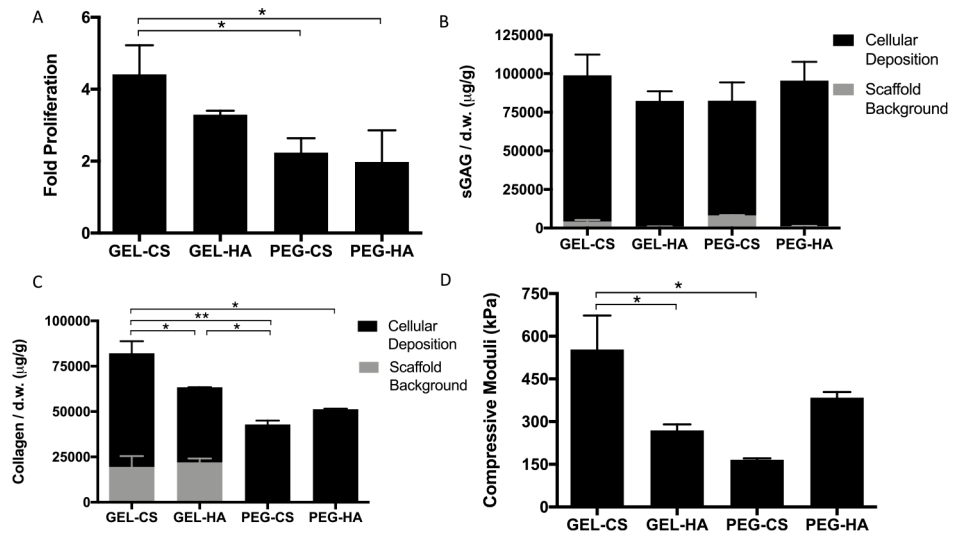
**Figure 2.**

Quantitative analysis of individual composition  $\mu$ RB scaffolds after 21 days in chondrogenic medium. (A) Fold change in proliferation from day 1. (B) sGAG and (C) collagen content in acellular and cellular scaffolds. (D) Compressive stiffness of gels. Data are mean  $\pm$  SD for  $n = 3$  samples. \* $p < 0.05$ ; \*\* $p < 0.001$ .

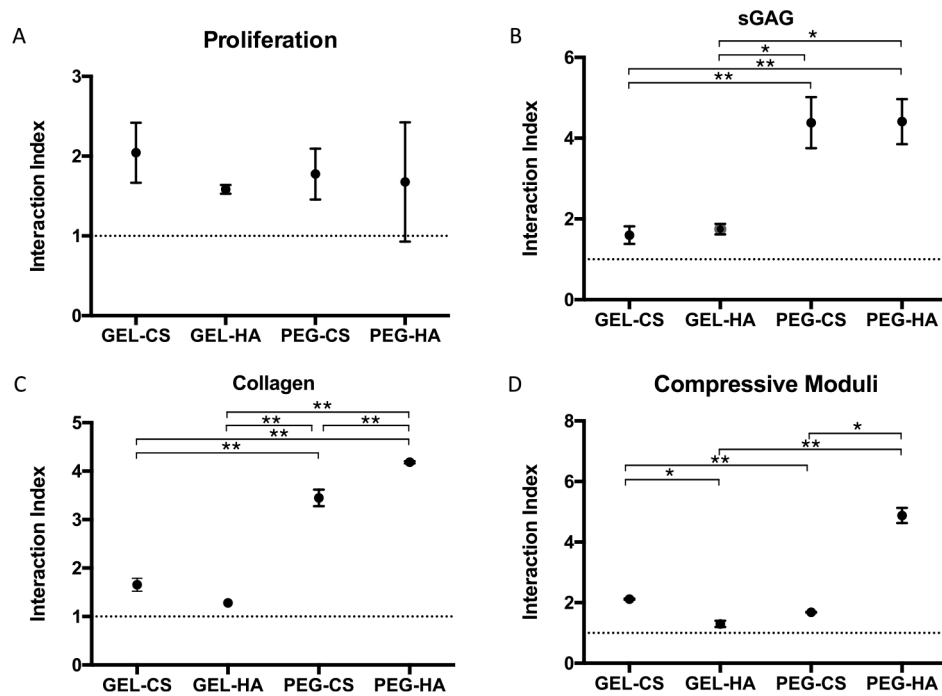


**Figure 3.** Histologic staining of constructs to visualize distribution of cartilage ECM deposition after 21 days in chondrogenic medium. (A) Safranin-O staining to visualize sGAG and (B) Masson's trichrome staining to visualize collagen. Immunostaining of (C) collagen II, articular cartilage marker, (D) collagen X, hypertrophic cartilage marker, and (E) collagen I, fibrocartilage marker. Scale bars: (A–B) 200 and (C–E) 100  $\mu\text{m}$ .

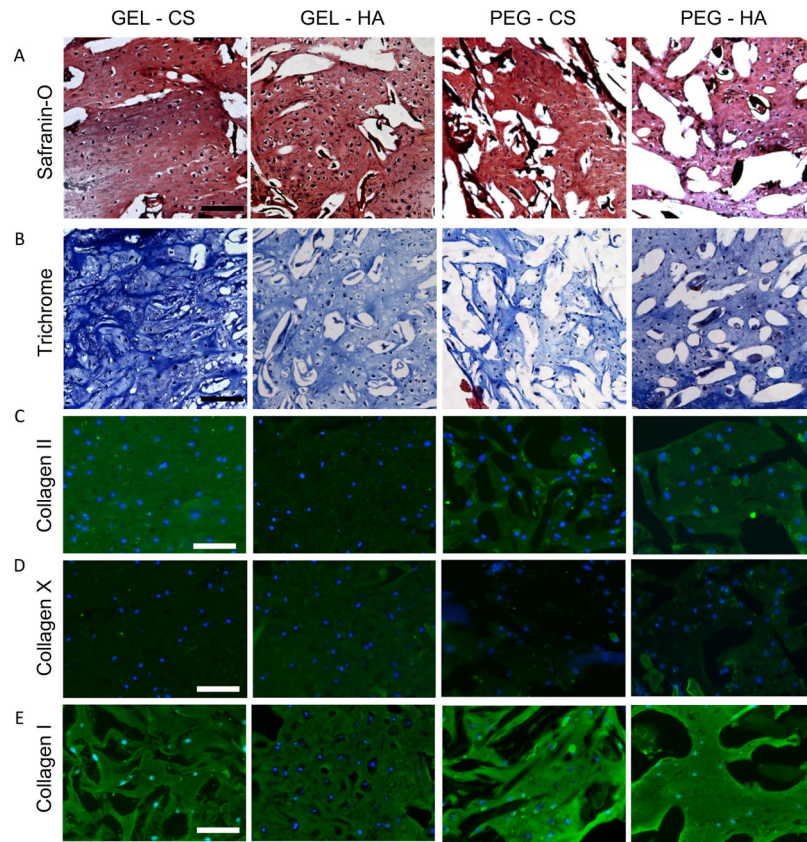




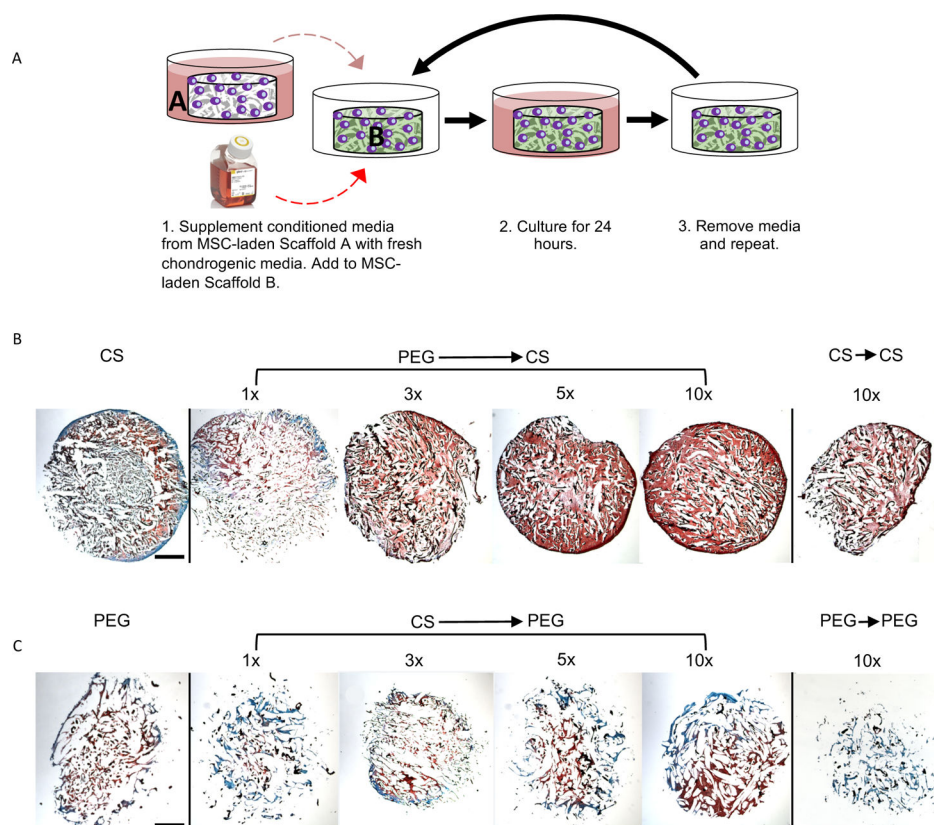
**Figure 4.** Quantitative analysis of mixed composition  $\mu$ RB scaffolds after 21 days in chondrogenic medium. (A) Fold change in proliferation from day 1. (B) sGAG and (C) collagen content in acellular and cellular scaffolds. (D) Compressive stiffness of gels. Data are mean  $\pm$  SD for  $n = 3$  samples. \* $p < 0.05$ ; \*\* $p < 0.001$ .



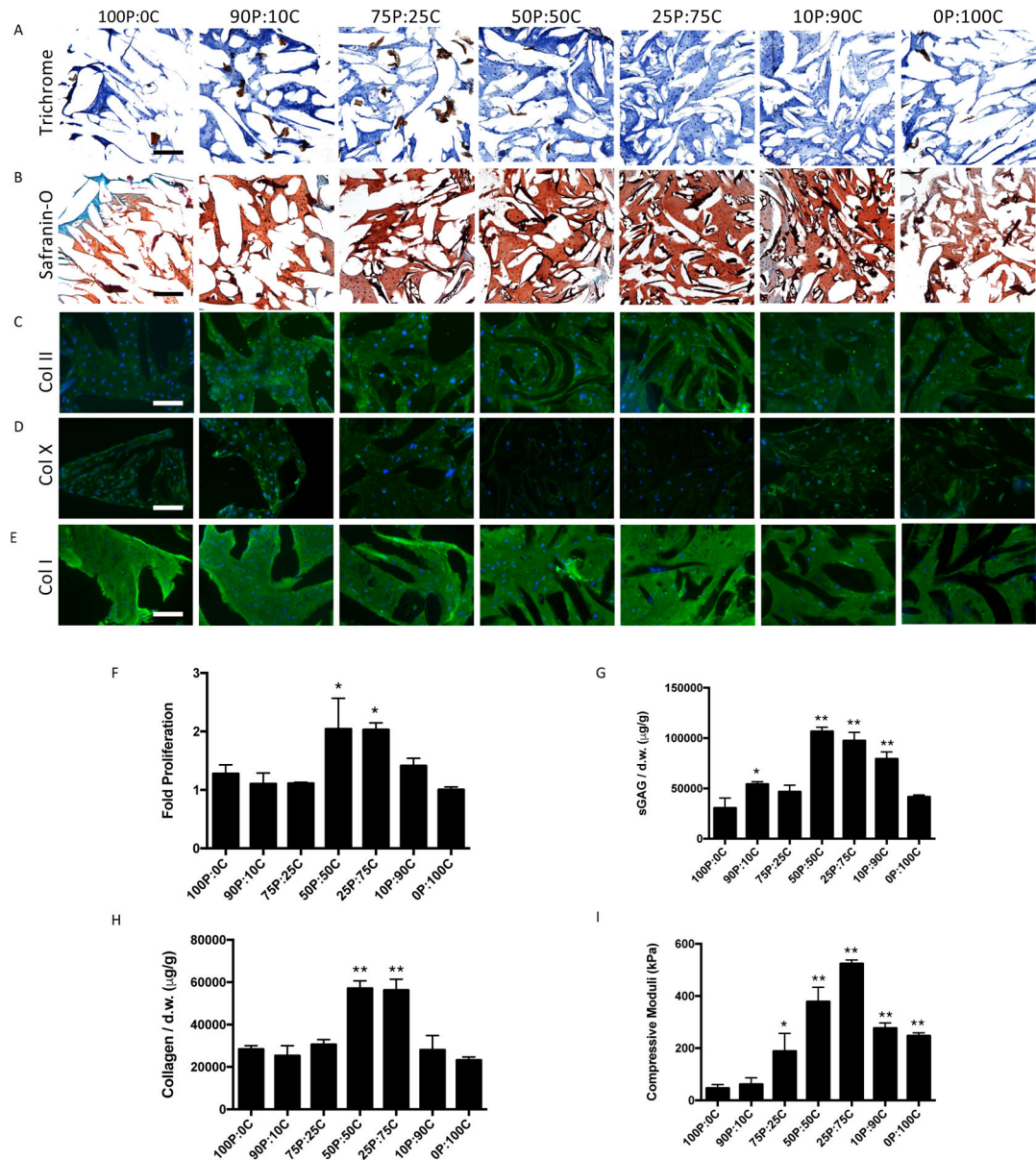
**Figure 5.** Interaction indices for (A) proliferation, (B) sGAG, (C) collagen, and (D) compressive moduli quantifying synergy in the mixed  $\mu$ RB constructs. Data are mean  $\pm$  SD for  $n = 3$  samples. \* $p < 0.05$ ; \*\* $p < 0.001$ .



**Figure 6.** Histologic staining of mixed  $\mu$ RB constructs after 21 days in chondrogenic medium to visualize distribution of (A) sGAG and (B) collagen. Immunostaining of (C) collagen II, articular cartilage marker, (D) collagen X, hypertrophic cartilage marker, and (E) collagen I, fibrocartilage marker. Scale bars: (A,B) 200 and (C-E) 100  $\mu$ m. n = 2 samples sliced and imaged for histology.



**Figure 7.** (A) Schematic of conditioned media experiment. Safranin-O staining after 21 days in chondrogenic medium of MSC-laden (B) CS and (C) PEG scaffolds cultured with conditioned media from MSC-laden PEG and CS scaffolds, respectively. 1× indicates concentrated conditioned media from 1 scaffold; 10× indicates concentrated conditioned media from 10 scaffolds. Scale bars: 1 mm. n = 2 samples sliced and imaged for histology.

**Figure 8.**

(A) Neocartilage production qualification (A–E) and quantitation (F–H) of MSCs in mixed PEG–CS  $\mu$ RB scaffolds with varying ratios after 21 days in chondrogenic medium. (A) Trichrome staining, (B) Safranin-O staining, (C) collagen II immunohistochemistry, (D) collagen X immunohistochemistry, and (E) collagen I immunohistochemistry. Biochemical analyses for (F) fold change of proliferation, (G) sGAG production, and (H) collagen production. (I) Compressive moduli of constructs. Scale bars: (A,B) 200  $\mu$ m and (C–E) 100  $\mu$ m. Data are mean  $\pm$  SD for n = 3 samples. \*p < 0.05; \*\*p < 0.001 compared to 100P:0C group. n = 2 samples sliced and imaged for histology.